RSC Advances

PAPER

View Article Online
View Journal | View Issue

Cite this: *RSC Adv.*, 2024, **14**, 38530

Investigation of a flexible, room-temperature fiber-shaped NH_3 sensor based on PANI–Au–SnO_2†

Qiuning Wang,‡[a] Yuan Peng,‡[a] Bin Guo,[b] Jianhai Sun,*[c] Yaxia Liu,*[d] Yanjun Wang[e] and Hongyan Zhang *[a]

A sensitive compound was successfully obtained by coating polyaniline (PANI) on the surface of composite nanoparticles consisting of Au-loaded tin dioxide, named as PANI–Au–SnO_2, using an *in situ* polymerization method. NH_3 sensors in thin-film and fiber-shaped forms were prepared by inkjet printing and impregnation methods, respectively, based on PANI–Au–SnO_2. The response characteristics of these NH_3 sensors developed from composite sensitive materials were investigated in detail. Results indicate an effective response of the sensors to NH_3 at room temperature. The thin-film sensor demonstrated a good linear relationship between the resistance change and NH_3 concentration within the range of 5–40 ppm, indicating its excellent repeatability and long-term stability. In comparison to the thin film sensor, the fiber-shaped sensor showed a consistently stable response to NH_3 even after 1000 cycles of repeated bending deformation. To demonstrate the practical application of the flexible fiber-shaped NH_3 sensor, a cap designed for NH_3 detection was fabricated by integrating the as-prepared sensor with a circuit board and an LED digital display. This assembly was incorporated into a commercially available ducktail cap, resulting in a wearable device capable of dynamically monitoring environmental NH_3 levels and displaying real-time values. This innovative application underscores the potential of these sensors in real-world scenarios, particularly in occupational safety, where workers might be exposed to harmful levels of NH_3. The cap could serve as a personal safety device, alerting the wearer to hazardous concentrations of NH_3, which is particularly relevant in industrial or agricultural settings.

Received 25th September 2024
Accepted 20th November 2024

DOI: 10.1039/d4ra06915c

rsc.li/rsc-advances

1. Introduction

Gas sensors are becoming essential in various fields, including medicine, industry, and defense. In particular, there is an urgent need to develop gas sensors that can operate at room temperature to monitor hazardous gas levels in the environment or indoor areas, especially in workplaces, to ensure human health and safety. Ammonia (NH_3) is one of the critical hazardous substances with a strong irritating odor and is widely used in chemical industries and other fields,[1] with millions of tons released into the atmosphere every year.[2,3] The concentration of NH_3 in the atmosphere is typically very low (1–5 ppb).[4] In indoor environments, the safety threshold for NH_3 concentration is considered to be below 0.2635 ppm, which is less than that in the industrial settings (39.53 ppm).[5,6] When inhaled at concentrations exceeding safe levels, NH_3 can be toxic and pose significant harm to humans due to its irritating and corrosive effects.[7–10] In addition, exhaled NH_3 serves as an important indicator of certain medical conditions .[11,12] Therefore, monitoring NH_3 is of great significance.

The development of room-temperature flexible NH_3 sensors is highly desired for wearable applications.[13,14] Developing NH_3 sensors with flexible and long-term stable operation remains a challenge. NH_3 sensors are widely used for dynamic monitoring of NH_3 concentration. In the field of smart wear, the performance of gas sensors has raised the bar for meeting practical application needs, which include room-temperature detection capability, lightweight nature, and flexibility.[15–17] Traditional rigid sensors, such as microelectromechanical systems (MEMS),[18–21] fail to meet these requirements, making the development of flexible NH_3 sensors essential. Metal oxide materials are often used in gas detection due to their resistance change when they encounter gas.[22] Metal oxides, such as zinc oxide (ZnO)[23–25] and tin oxide (SnO_2),[26,27] were the earliest materials used for detecting NH_3. Among these materials, SnO_2 is appealing due to its low cost, low toxicity, ease of

[a]*Beijing Key Laboratory of Clothing Materials R&D and Assessment, Beijing Engineering Research Center of Textile Nanofiber, Beijing Institute of Fashion Technology, Beijing, 100029, P. R. China. E-mail: zhyzzh@126.com*

[b]*Zhongshan Institute of Changchun University of Science and Technology, P. R. China*

[c]*State Key Laboratory of Transducer Technology, Aerospace Information Research Institute, Chinese Academy of Sciences, Beijing, 100194, P. R. China*

[d]*School of Fashion, Beijing Institute of Fashion, China*

[e]*Beijing Institute of Fashion Technology, School of Fashion Flat Knitting Machine Lab, China*

† Electronic supplementary information (ESI) available. See DOI: https://doi.org/10.1039/d4ra06915c

‡ Both authors contribute equally to this work.

manufacture, and excellent sensitivity. However, its gas detection requires high temperature, making it unsuitable for wearable applications.[28] For this reason, researchers have made numerous attempts to find alternatives, with organic–inorganic composites attracting much attention. Conductive polymers, which combine the mechanical properties of polymers with metal-like electrical properties, are important materials in the field of smart wearables.[29–32] Among the conductive polymers, polyaniline (PANI) is one of the most promising materials for detecting NH_3 at room temperature. When PANI is used to sense NH_3, it offers the advantages of a rapid response and stable performance.[33] However, there are still issues with its sensitivity, processability, and so on.[34–38] Therefore, composites of metal oxides and conductive polymers have been investigated as they could offer significant advantages as NH_3-sensitive materials.[39,40] Indeed, many composites consisting of metal oxides and conducting polymers have been developed as NH_3 sensors and have demonstrated excellent sensing performance. For example, Siqi Li[41] *et al.* prepared SnO_2–PANI nanocomposites with a well-defined microstructure and large specific surface area. The response speed of 20 mol% SnO_2–PANI to 100 ppm NH_3 at room temperature was 6.2 times higher than that of the sensor based on PANI alone. Additionally, it could detect low concentrations with outstanding selectivity. In addition, doping precious metals, such as Au and platinum, as well as other nanoparticles, into metal oxides can effectively enhance the gas-sensing properties.[42,43] For example, Manish Deshwa[44] and others have prepared 3% v/v Au-doped ZnO thin films for use as acetone sensors. Compared to the undoped thin films, they found the response was significantly improved, exhibiting very high sensitivity, a rapid response and recovery time, and a lower optimal working temperature.

In the present study, we employed the wet impregnation method and *in situ* polymerization method to prepare sensitive materials of PANI–Au–SnO_2 and utilized these materials to fabricate sensor devices. It was found that fine-tuning the properties of the composites could directly affect the sensitivity, selectivity, response time, and recovery time of the NH_3 sensors. These sensors were evaluated to assess not only their electrical response to NH_3 exposure but also their mechanical durability, long-term stability under various environmental conditions, and the repeatability of the response. Smart sensor devices were developed that were highly sensitive and selective to NH_3, as well as durable enough to be utilized in flexible and wearable applications, which could help protect human health in potentially dangerous environments. The innovative approach used in this study reflects the increasing trend in sensor development to create multifunctional, reliable, and user-friendly devices for environmental monitoring and personal safety.

2. Experimental

2.1 Materials

Aniline, ethanol, and terpineol were purchased from Tianjin Damao Chemical Reagent Factory. Nano-SnO_2 was purchased from Hebei Yi Gui Welding Materials Co., Ltd. Chloroauric acid ($HAuCl_4 \cdot 3H_2O$) was purchased from Shanghai McLean Biochemical Technology Co., Ltd. Ammonium persulfate (APS) was purchased from Beijing Tong Guang Fine Chemical Co., Ltd. Concentrated NH_3 water was purchased from Tianjin Guang Fu Technology Development Co., Ltd. Hydrochloric acid (HCl) was purchased from Saan Chemical Technology (Shanghai) Co., Ltd. Conductive silver ink was purchased from Shenzhen Saya Electronic Paste Co., Ltd. The e-PTFE waterproof breathable film was purchased from Polyfluorine New Material Technology Co., Ltd. Polydimethylsiloxane (PDMS) was purchased from Dow Corning, USA. The chemical reagents mentioned above were all analytically pure and were used as-received without further purification.

2.2 Preparation of the composite sensing materials

2.2.1 Preparation of Au–SnO_2. First, 20 nm SnO_2 nanospheres and $HAuCl_4 \cdot 3H_2O$ were added to 20 mL of ethanol and stirred magnetically. The mixture was then heated to 40 °C and allowed to evaporate completely. The mixture was then transferred to a crucible and calcined in a muffle furnace at 300 °C for 2 h to obtain Au–SnO_2 (Fig. 1(a)).

2.2.2 Preparation of PANI–Au–SnO_2. Solution A was prepared by adding 1.14 g of APS to 15 mL of 1 M HCl and stirring continuously for 30 min, and was then placed in an ice water bath. A specific quantity of Au–SnO_2 was added to 15 mL of 1 M HCl and dispersed using ultrasonication. Subsequently, 10 mmol of aniline monomer was added and sonication was continued for 30 min, and then cooled to obtain solution B. Solution A was slowly added to solution B to obtain PANI–Au–SnO_2. This was then left standing for 3 h resulting in a layered dark-green suspension, which was then vacuum filtered, and the obtained sample was washed with ethanol and deionized water. The collected material was placed in a drying oven at 80 °C and then ground into powder for use in sealed equipment (Fig. 1(b)).

The material was generally denoted as PASn*x*A*y*, where PA, Sn, and A represent PANI, SnO_2, and Au, respectively, *x* represents the molar percentage of SnO_2 (mol%), and *y* represents

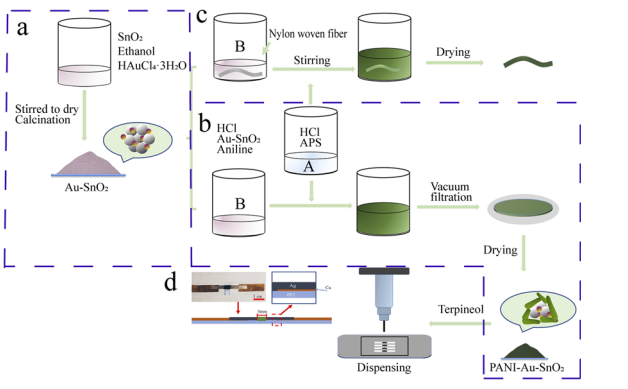

Fig. 1 Preparation of gas-sensitive materials and ammonia gas sensors. (a) Fabrication of Au–SnO_2 material. (b) Fabrication of PANI–Au–SnO_2 compound. (c) Preparation of the fiber-shaped sensor. (d) Fabrication of the thin film sensor.

that of Au (at%), respectively. For the different samples, the number before Sn represents the particle size of SnO_2; for example, PA20Sn20A2, indicates 20 nm-sized SnO_2, and 20 mol%, Au addition of 0.02 g.

2.3 Preparation of the flexible NH_3 sensor

The preparation process of the flexible sensor is shown in Fig. 1(c) and (d). First, 0.05 g of the sensitive material and an appropriate amount of terpineol were ground together evenly. This mixture was applied to a wide electrode (2 mm) printed by conductive silver ink and placed in an oven to dry at 80 °C for 2 h to obtain the thin film sensor (Fig. 1(d)). Meanwhile, a 3 cm nylon braid was added to solution B during the preparation of the PANI–Au–SnO_2 to obtain a fiber-shaped flexible NH_3 sensor. The other steps were the same as for the preparation of PANI–Au–SnO_2 (Fig. 1(c)).

2.4 Sample characterization

A drying oven (DZF-60030v, China), ultrasonic machine (DS2510DTH, China), muffle furnace (SX-B01123, China), and magnetic stirrer (DF-101S, China) were utilized in the preparation of the materials and sensors. The morphology, microstructure, and particle-size distribution of the NH_3-sensitive materials were characterized by scanning electron microscopy (SEM, JSM7500F, JEOL, Japan). The elements of NH_3 sensitive materials were elucidated through transmission electron microscopy (TEM, JEM-2100F, JEOL, Japan), X-ray photoelectron spectroscopy (XPS, ESCALAB 250 Xi, Thermo Fisher Scientific, USA), and element analysis using energy dispersive spectroscopy (EDS, S-4800). The crystal structure was characterized by polycrystalline X-ray diffractometry (XRD, D8 Focus, Bruker, Germany). The chemical functional group information of the samples was characterized by Fourier transform infrared spectrometry (FTIR, IRPrestige-21, SHIMADZU, Japan). The sensor was tested for NH_3 sensing using a self-made gas test system (Fig. S1†). During NH_3 testing, the resistance of the gas sensors was measured using a data acquisition and recording multimeter system (DAQ6510, Keithley, USA). The cyclic bending performance of the sensor was tested at room temperature using a stepper motor with a lead of 2 cm and a module (Fig. S2†), and the resistance change was tested in real-time with a DAQ6510 system.

2.5 Gas-sensing measurements

The gas responses of the prepared sensors were tested by the device shown in Fig. S1.† The device consisted of a closed box, DAQ6510, and a notebook computer. The specific test method involved placing the sensor in the closed box and connecting the DAQ6510. When the resistance value displayed on the computer was stable, the closed box was filled with a predetermined amount of gas to be tested, and the resistance value was measured until it became stable. Then, the closed box was opened, causing the stable resistance value to change, and this was again measured until it became stable, thus completing the test.

In this study, two concentration techniques for producing NH_3 were employed. Initially, the static testing method was utilized. Given that concentrated NH_3 water and NH_3 are corrosive, to protect the mass flowmeter from damage, we implemented the static testing method, where a specific concentration of NH_3 was generated through the evaporation of the concentrated NH_3 water. The detailed procedure involved connecting conductive tape at both ends of the flexible sensor to the DAQ instrument, and then recording the resistance value of the NH_3 gas sensor in real time. During the experiment, the heating stage was maintained at 80 °C to expedite NH_3 evaporation. Simultaneously, the slide was positioned on the heating stage, and 4 μL of concentrated NH_3 water was added dropwise. Subsequently, the flexible sensor and the slide with NH_3 water were enclosed in a transparent box with a volume of 3000 mL, creating a simple test environment of 600 ppm NH_3 concentration to initially evaluate the prepared sensitive materials. The formula for generating NH_3 gas is as follows:[45]

$$Q = (V \times C \times M)/(22.4 \times d \times \rho) \times 10^{-9} \times (273 + T_r)/(273 + \mathrm{TB})$$

where Q is the volume of the liquid to be taken (mL), V is the volume of test container (mL), M is the molecular weight of the substance (g), ρ is the purity of the liquid, C is the concentration of the gas to be prepared (ppm), d is the liquid density (g cm^{-3}), and T_r is the test environment temperature (°C).

The second methodology was the gas-distribution procedure, which involved diluting a defined concentration of standard NH_3 within a specified volume solvent bottle to establish the necessary test concentration. This technique evaluated the subsequent performance of the selected materials and devices, demonstrating optimal functionality. The experimental processing steps were the same as those in the static test method.

The sensitivity of a gas sensor is a measure of its ability to change its resistance in the presence of a target gas. It is defined by the ratio of the resistance of the sensor in a specific gas (R_g) to the resistance of the sensor in air (R_a). The sensitivity is generally expressed by S, where $S = R_g/R_a$. The response and recovery time are the intervals needed for the sensor to reach the total resistance change upon exposure to the target gas (response time), and then return to 90% of the baseline when the gas is removed (recovery time), respectively. Here, standard NH_3 was diluted to obtain the required concentration of NH_3 for testing, and the real-time resistance was measured using a digital multimeter system. The above tests were carried out at room temperature (25 °C) except for the test to determine the influence of temperature.

3. Results and discussion

3.1 Optimizing of the NH_3-sensitive materials

To optimize the material ratio, the particle size and dosage of SnO_2, and the Au doping amount were carefully selected. The size of SnO_2 particles has a significant impact on the doping efficiency of Au; therefore, sizes of 10, 20, and 50 nm were tested. The doping adjustment of Au was determined by the quantity of chloroauric acid, specifically 0.02, 0.04, and 0.08 g.

The PN junction formed by the P-type PANI and N-type SnO_2 is crucial for the NH_3 sensor to have good sensing performance. In the experiment, we compared three different SnO_2 contents, and the testing was carried out at room temperature, with a relative humidity of 44% and an NH_3 concentration of 600 ppm (Fig. S3†). The response value for each material combination was measured and documented using the testing system (Fig. S1†). Fig. S3† shows the gas-sensing results of the sensing materials prepared by changing the doping amounts of nanoparticles and the doping amount of gold with the doped SnO_2 nanoparticles of different diameters of 10, 20, and 50 nm, respectively. From Fig. S3a,† we can see that irrespective of the composite material, the response value was less than 2.5, which was worse than the sensing effect of pure PANI. It can be seen from Fig. S3b† that the sensing effect of PA20Sn20A2 was significantly higher than that of the other materials, and the response value was above 2.7. Fig. S3c† shows that the response value of the composite material of SnO_2 nanoparticles with a particle size of 50 nm was lower than 2.0, which was significantly lower than the others. Therefore, the doping amount of SnO_2 was fixed at 20 mol%, and then sensors were prepared by changing the particle size of SnO_2 nanoparticles and the doping amount of Au, and the response values were tested and compared (Fig. 2). The data in Fig. 2 suggest that the combination designated as PA20Sn20A2, which corresponded to PANI with 20 nm SnO_2 particles and Au doping amount with 0.02 g of chloroauric acid, exhibited the highest response at 600 ppm for NH_3. The identification of PA20Sn20A2 as the material with the highest response indicates that this composite had the most suitable combination of particle size and doping level for the detection of NH_3 under the tested conditions.

3.2 Characterization of the NH_3-sensitive material

The morphology of NH_3-sensitive material was characterized using SEM, as shown in Fig. 3. The SEM of 20 nm SnO_2 (Fig. 3(a)) revealed spherical nanoparticles with a loosely arranged porous structure between them. This structure effectively increases the specific surface area, making it more conducive to the adsorption and diffusion of gas. Fig. 3(b) displays the 20 nm SnO_2–PANI composite, where it can be seen that PANI was wrapped around the SnO_2, forming a nanofibrous structure that was interconnected into a mesh structure with a diameter of about 100–200 nm. Fig. 3(c) shows the SEM image of 20 nm SnO_2 doped with a small amount of Au, and the microscopic morphology was similar to that of undoped SnO_2. Fig. 3(d) presents the SEM of the PA20Sn20A2 composite material. It is evident from the figure that PA20Sn20A2 had a looser porous and three-dimensional network structure, which could improve the sensitivity of the NH_3 sensor.

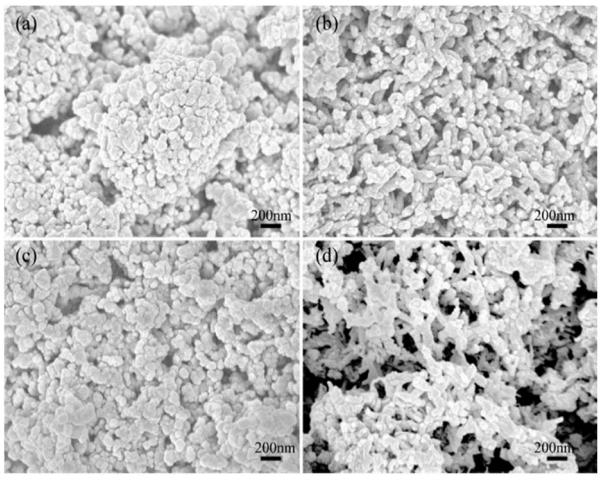

Fig. 3 SEM images of the NH_3 sensitive material. (a) 20 nm SnO_2; (b) PA20Sn; (c) 20SnA2; (d) PA20Sn20A2.

XRD and EDS were used to characterize the composition of the material. The XRD pattern in Fig. 4(a) shows the phase and crystal structure of the material. The original PANI exhibited a diffuse diffraction peak between 20–35°, indicating an amorphous phase structure. However, there were also small diffraction peaks present at 50–60°, which could be attributed to impurities. These impurities were confirmed by comparing the XRD curve of pure SnO_2 with the standard card of rutile SnO_2 (JCPDS: 41-1445), which showed no other impurity peaks. The diffraction peaks of each component in the material exhibited noticeable changes in intensity. When comparing the Au-doped

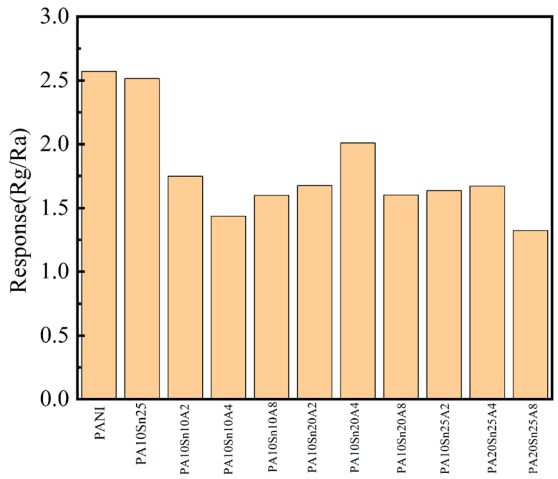

Fig. 2 Response values of different NH_3-sensitive materials to 600 ppm NH_3 (from left to right is PANI, PA10Sn25, PA10Sn10A2, PA10Sn10A4, PA10Sn10A8, PA10Sn20A2, PA10Sn20A4, PA10Sn20A8, PA10Sn25A2, PA20Sn25A4, PA20Sn25A8).

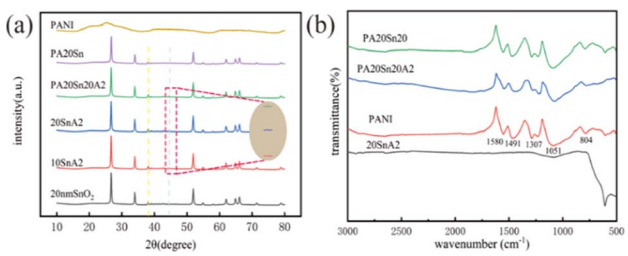

Fig. 4 (a) XRD curves of the NH_3-sensitive materials. (b) Infrared spectra of the NH_3-sensitive materials.

material with the undoped material, a small diffraction peak was observed at approximately 45°, but it was not prominent, indicating a low level of Au doping. Energy spectral analysis of PA20Sn20A2 and 20Sn20A2 (Fig. S4†) was conducted separately. However, due to the small amount of Au present, the corresponding peak may have been obscured by other peaks, making it difficult to detect the presence of Au. The specific element contents in the two materials can be found in Table 1 and Table S1.† Furthermore, From Fig. S5 and Table S2,† it can be seen that the XPS analysis of PA20Sn10Au2 verified the trace presence of Au.

The FTIR spectral characterization was conducted on four materials, namely the pure PANI, PA20Sn20, PA20Sn20A2, and 20SnA2. The wave number range of 4000–500 cm^{-1} was used to discern the chemical bonding interactions present in the nanocomposites. Fig. 4(b) shows the main characteristic absorption peaks of PANI, which were located at 1580, 1491, 1307, 1051, and 804 cm^{-1}. The absorption peaks at 1580 and 1491 cm^{-1} corresponded to the C=C stretching vibration of the quinone ring (N=Q=N) and the benzene ring (N–B–N), respectively. The absorption peak at 1307 cm^{-1} was attributed to the C–N stretching vibration. The peaks at 1051 and 791 cm^{-1} represented the in-plane and out-of-plane bending vibrations of the benzene ring C–H, respectively. When comparing the IR spectra of PANI with PA20Sn20 and PA20Sn20A2, it could be observed that the characteristic absorption peaks of PA20Sn20 and PA20Sn20A2 were shifted to higher wave numbers. This shift was caused by the effect of SnO_2 on PANI when it was compounded with SnO_2.

3.3 Characterization of the thin film sensor

Fig. 5(a) shows the real-time response curves of the thin film sensor based on the PA20Sn20A2 material at various concentrations of NH_3 (5–40 ppm) at room temperature. The sensor displayed a rapid increase in resistance upon exposure to NH_3, stabilizing at 400–500 s. When fresh air was introduced, the resistance gradually decreased back to the initial value. However, it can be seen from the figure that the sensor resistance value did not fully recover after the gas concentration was greater than 30 ppm. This is because the test process was a continuous test, resulting in the sensor not being completely desorbed. At 20 ppm NH_3, the thin film sensor exhibited a response time of 93 s and recovery time of about 168 s (Fig. 5(b)). The resistance of the sensor increased with the NH_3 concentration, showing a larger response at higher

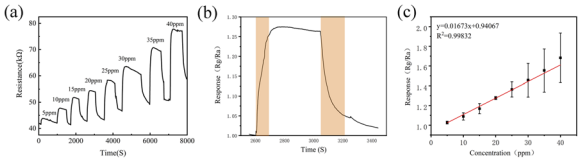

Fig. 5 Response properties of the thin film NH_3 sensor based on the PA20Sn20A2 material at room temperature. (a) Dynamic response curve of the sensor to NH_3 with a concentration of 5 to 40 ppm. (b) Response recovery curve of the sensor at 20 ppm NH_3 concentration. (c) Response and linear fitting curves for various concentrations of NH_3. Error bars represent the standard deviations obtained from at least three independent measurements.

concentrations, with a maximum response of 1.68 at 40 ppm NH_3. Post 6000 s and exposure to 35 ppm, and 40 ppm NH_3 concentration, the thin film sensor resistance could not return to its initial value. This may be due to the prolonged exposure causing NH_3 molecules to spread and react with the sensitive material inside, which means they may not have completely desorbed, and instead reacted.

Fig. 5(c) is a linear fitting curve based on the response of the thin film sensor at different concentrations of PA20Sn20A2 at room temperature, and each concentration was tested three times. A linear relationship was found between the response and the correlation of the sensor. The correlation coefficient was 0.99832, indicating a highly accurate and reliable sensor performance.

3.4 Characterization of the fiber-shaped sensor

The flexibility of a sensor is crucial for a comfortable wearing experience. This can be measured by its ability to bend to a certain degree. We conducted bending experiments on two thin film NH_3 sensors using a stepper motor with a lead of 2 cm and a module (Fig. S2†). The thin film displayed serious damage after only a few bends, as some of the NH_3-sensitive materials began to fall off from the PET substrate. To avoid this issue, we prepared a flexible fiber-shaped NH_3 sensor using a nylon woven line as the substrate. Fig. S6† shows SEM photos of the fiber-shaped NH_3 sensor with different magnifications. The nylon braided line was made up of multiple 15 μm nylon fibers, coated with PA20Sn20A2. In Fig. 6(a), we can see the response of the fiber-shaped NH_3 sensor at a concentration of 10–40 ppm. The illustration shows an optical image of the fiber-shaped flexible NH_3 sensor, which measured 30 × 3 × 2 mm and had

Table 1 Elemental analysis of PA20Sn20A2

Element	Concentration of element	Intensity correction	Percentage by weight	Percentage by weight sigma	Atomic percent ratio
C K	4.90	1.0015	43.61	0.83	68.16
O K	1.02	0.4374	20.84	0.74	24.45
S K	0.23	1.0642	1.91	0.08	1.12
Cl K	0.25	0.8770	2.55	0.10	1.35
Sn L	2.71	0.7799	31.08	0.58	4.92
Total			100.00		

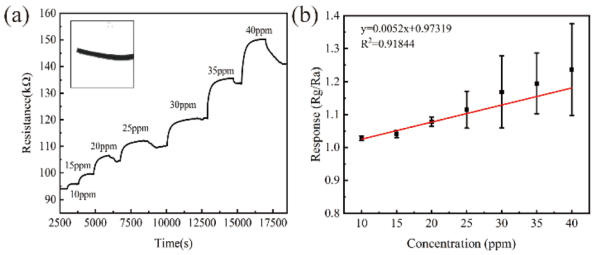

Fig. 6 (a) Dynamic response curve of the NH_3 sensor to different concentrations (10–40 ppm) of NH_3, as illustrated by the optical image of the 30 mm fiber-shaped NH_3 sensor. (b) Response and linear fitting curves for various concentrations of NH_3. Error bars represent the standard deviations obtained from at least three independent measurements.

a dark-green PANI coating. Despite its smaller size, the fiber-shaped NH_3 sensor could still maintain a good response. In Fig. 6(b), we can see the response of the sensor at different NH_3 concentrations and its linear fitting relationship with a correlation coefficient of 0.92. Due to the lower amount of NH_3-sensitive material on the fiber, its response was not as strong as the thin-film NH_3 sensor.

We tested the response of the fiber-shaped sensor to various gases at room temperature, and the results are shown in Fig. 7(a). The responses to CO, H_2S, NO_2, NH_3, SO_2, and H_2 equaled 1.04, 1.05, 1.00, 1.12, 0.10, and 0.20, respectively. It can be seen from the figure that the response value of the sensor to NH_3 was higher than that of other interfering gases, which proved that the sensor had good selectivity to NH_3 at room temperature.

The continuous and stable response of the gas sensor to the target gas is also a very important performance. In Fig. 7(b), it can be seen that the fiber-shaped sensor was allowed to respond three times continuously to 40 ppm NH_3 at room temperature to obtain a real-time resistance change curve. The analysis confirmed that the continuous response of the sensor to 40 ppm NH_3 was relatively stable.

The stability of the fiber-shaped sensor was characterized by various factors, including temperature, curvature, humidity, and

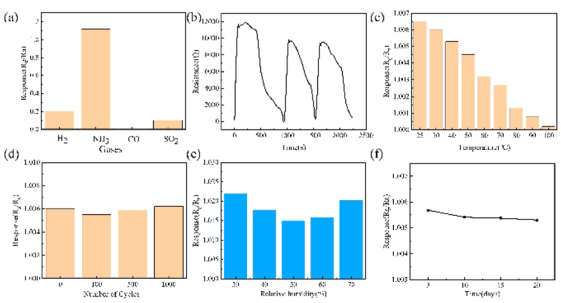

Fig. 7 (a) Response of fiber-shaped sensor towards different interference gases with a concentration of 40 ppm. (b) Cycling response toward 40 ppm NH_3 at room temperature. (c) Response value of the NH_3 sensor at different operating temperatures. (d) Response changes of NH_3 sensors after different bending cycles. (e) Response values of the NH_3 sensor at different relative humidities. (f) Temporal stability of the NH_3 sensors.

time, at a concentration of 10 ppm NH_3. Fig. 7(c) shows the response of the sensor under different temperatures. As the ambient temperature increased, the sensor response value decreases from 1.0065 at 25 °C to 1.0002 at 100 °C. This indicates that the optimal operating temperature for this sensor was near room temperature. Fig. 7(d) shows the response of the sensor to NH_3 after various bending cycles, and the results indicate that the response slightly improved and remained around 1.006, demonstrating excellent bending stability. This may be due to the increased porosity of the sensitive material during bending. Fig. 7(e) shows the effect of humidity on the sensor's response. From the results for the thin film sensor, it was obvious that the sensor response was affected by higher humidity. To combat this, an e-PTFE was covered on the sensor and sealed with PDMS on the end. When the humidity was as high as 70%, the response of the sensor was only 0.2% lower than that at 30% humidity. Even at 50% humidity, which was the most obvious decrease shown in the figure, the decrease was only 0.7% (Fig. 7(e)). This indicates that the e-PTFE helped the sensor resist the effects of humidity. Fig. 7(f) illustrates the change in sensor response value over time, indicating a decrease of 0.04% after 20 days of storage at room temperature. This result fell within the acceptable range and demonstrated good time stability. Table S3† presents a brief comparison of the performance of our NH_3 sensor with other sensors. Compared with other room-temperature NH_3 sensors, our PANI–Au–SnO_2 sensor showed faster response and recovery times for lower concentrations of NH_3 at room temperature. In addition, the sensor based on PANI–Au–SnO_2 also had a higher response value than other sensors, indicating that this composite-based sensor could be applied for the potential monitoring of NH_3 at room temperature.

3.5 Practical application

We fabricated a small PCB circuit board (Fig. S9(a)†) for data monitoring, which was connected to the fiber-shaped sensor and powered by a lithium battery. It could transmit real-time detected NH_3 data to a mobile terminal or a computer terminal through Bluetooth. The sensing system depicted in Fig. S9(a)† was incorporated into the duck tongue cap *via* needle stitching, and the exposed circuit was refined with wool felt. Consequently, the NH_3-sensing duck tongue cap illustrated in Fig. S9(b)† was successfully fabricated. The cap was inserted into the testing apparatus and then NH_3 was introduced. The LED display indicated the relative concentration of the NH_3. Fig. S9(c)† presents the circuit schematic of the whole system. The duck tongue cap could be expected to be used in the future to protect workers in NH_3-working environments all year round so that workers could timely understand whether the NH_3 level in their environment is safe.

3.6 Gas-sensing mechanism

The conductive polymer PANI and its doped materials play a crucial role in the NH_3 sensor. The sensitivity of the sensor was mainly attributed to the protonation and deprotonation process of PANI, which is reversible (Fig. 8(b)). This characteristic ensures that the sensitive material prepared using PANI

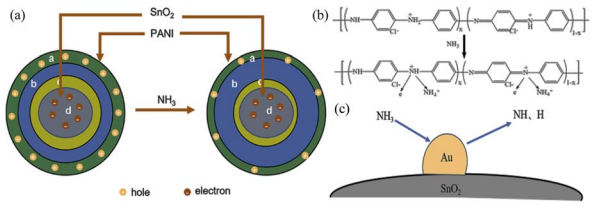

Fig. 8 (a) Mechanism diagram of the PANI–SnO_2 sensitive material. (b) Mechanism of the sensitivity of PANI to NH_3. (c) Facilitating effect of Au to the NH_3 response.

can repeatedly offer NH_3 detection. Initially, PANI is non-conductive, but when it is doped with acid, it becomes polarized and has a dual-polarized structure, making it conductive. When the sensor is exposed to NH_3, the proton acid doped in PANI reacts with NH, resulting in the formation of NH_4^+. This reaction causes PANI to change from a doped conductive aniline salt state to a non-conductive aniline alkali state, leading to a significant increase in resistance. However, when the NH_3 atmosphere is removed and the sensor is placed in fresh air, NH_4^+ decomposes into NH_3 and H^+. The H^+ then participates in PANI again, transforming it into an aniline salt state and reducing the resistance, thereby restoring the conductivity.[45,46] The gas-sensing properties of the Au-doped SnO_2 composite PANI material were significantly improved. This improvement could be attributed to the formation of a p–n heterojunction between the p-type PANI and n-type SnO_2, as well as the catalytic properties of the noble metal Au. The presence of a p–n heterojunction has been shown to greatly enhance the sensitivity of sensitive materials to NH_3.[47–49] When PANI is composited with SnO_2 during the acidification process, it forms a core–shell structure on the surface of SnO_2 nanospheres, as described in Fig. 8(a). In the presence of air, the holes of $PANIH^+$ and the electrons of SnO_2 nanospheres diffuse toward the middle, creating a depletion layer at the interface between the two materials (regions b and c in Fig. 8). This depletion layer leads to an increase in resistance. However, in the presence of air, the depletion layer is relatively narrow, resulting in a high conductivity and low resistance of the sensitive material. When the sensor is exposed to NH_3, the NH_3 captures H^+ ions in $PANIH^+$, causing PANI to convert from an emerald salt to emerald alkali. This reduces the number of holes, resulting in a wider depletion layer (region b), which significantly increases the resistance.[50,51] The enhancement of performance by precious metals is mainly due to the spillover mechanism of these metals, which possess catalytic properties.[52–54] On the one hand, the presence of Au increases the contact between the material and the reducing gas, increasing the specific surface area of the sensitive material and improving the performance of the NH_3 sensor. Additionally, Au acts as a catalyst for surface catalytic activity. NH_3 molecules diffuse on the surface of Au and adsorb onto it. The p orbital of NH_3 interacts with the d orbital of the Au atom, producing a highly reducible hydrogen atom. This promotes the reaction of PANI.[55–57] The process is illustrated in Fig. 8(c). Therefore, Au can effectively improve the performance of the material.[58–60]

4. Conclusions

In summary, a new flexible NH_3 sensor based on PANI–Au–SnO_2 was successfully developed. We prepared a sensitive material of a PANI composite loaded with Au–SnO_2 through *in situ* polymerization. Thin-film and fiber-shaped NH_3 sensors were then prepared using a printing, coating, and impregnation method, respectively. The p–n heterojunction formed between PANI and SnO_2 along with the catalytic effect of Au significantly improved the gas-sensing performance of the NH_3 sensor. Both sensors showed good responses in the range of 5–40 ppm of NH_3 at room temperature. The compactness, flexibility, lightweight, and good stability of the fiber-shaped NH_3 sensor make it suitable for wearable NH_3-sensing applications. Additionally, the NH_3-monitoring system addressed the issues faced by traditional electrical signal monitoring methods and provides a solution for the entire process from preparation to application. We integrated the fiber-shaped NH_3 sensor on a duck tongue cap and linked this to a display screen to display the NH_3 content in the environment in real-time, providing a certain safety guarantee for workers working in the NH_3 environment, which is expected to become an important part of the application of wearable devices. However, the high error rates of the fiber-shaped NH_3 sensor necessitate some subsequent operations to enhance the sensor precision. Future advancements in fiber preparation and post-processing methods could be anticipated to enhance the sensor performance.

Data availability

The data supporting this article are included in the ESI.†

Author contributions

Qiuning Wang: conceptualization, data curation, investigation, methodology, writing–original draft. Yuan Peng: conceptualization, data curation, investigation, methodology, writing–original draft. Bin Guo: electrical guidance. Jianhai Sun: performance characterization of the sensor. Yaxia Liu: textile design guidance. Yanjun Wang: textile production. Hongyan Zhang: overall planning and guidance.

Conflicts of interest

There are no conflicts to declare.

Acknowledgements

This work was supported by the National Key Research and Development Plan of China (Grant No. 2022YFB3805804, Grant No. 2022YFB3805802), Classified Development of Municipal Colleges and Universities – the Project of Constructing the Emerging Interdisciplinary Platform Based on "Clothing Science" of Beijing Institute of Fashion Technology (Grant No. 11000024T000003073871), the Beijing Scholars Program (Grant No. RCQJ20303) and the Graduate Student Research and

Innovation Program of Beijing Institute of Fashion Technology (Grant No. X2024-049).

References

1 D. Kwak, Y. Lei and R. Maric, NH_3 sensors: a comprehensive review, *Talanta*, 2019, **204**, 713–730.
2 B. Timmer, W. Olthuis and A. V. D. Berg, Ammonia sensors and their applications-a review, *Sens. Actuators, B*, 2005, **107**, 666–677.
3 Y. Zeng, S. Tian and Y. Pan, Revealing the Sources of Atmospheric Ammonia: A Review, *Curr. Pollut. Rep.*, 2018, **4**, 189–197.
4 G. K. Mani and J. Rayappan, A highly selective room temperature NH_3 sensor using spray deposited zinc oxide thin film, *Sens. Actuators, B*, 2013, **183**, 459–466.
5 *Standards for Indoor Air Quality*, State Administration for Market Regulation of the People's Republic of China, GB/T 18883-2022.
6 *Hygienic standards for the design of industrial enterprises*, China's Occupational Health Standards Committee of the Ministry of Health, GBZ1-2010.
7 G. K. Mani and J. Rayappan, A highly selective and wide range ammonia sensor—nanostructured ZnO: Co thin film, *J. Mater. Sci. Eng. B*, 2014, **191**, 41–50.
8 M. S. Yarandi, M. Mahdinia, J. Barazandeh and A. Soltanzadeh, Evaluation of the toxic effects of ammonia dispersion: consequence analysis of ammonia leakage in an industrial slaughterhouse, *Med. Gas Res.*, 2021, **11**(1), 24–29.
9 Y. Li, H. T. Ban and M. J. Yang, Highly sensitive NH_3 gas sensors based on novel polypyrrole-coated SnO_2 nanosheet nanocomposites, *Sens. Actuators, B*, 2016, **224**, 449–457.
10 H. Y. Li, C. S. Lee, D. H. Kim and J. H. Lee, Flexible room-temperature NH_3 sensor for ultrasensitive, selective, and humidity-independent gas detection, *ACS Appl. Mater. Interfaces*, 2018, **10**(33), 27858–27867.
11 P. Španěl and D. Smith, What is the real utility of breath NH_3 concentration measurements in medicine and physiology, *J. Breath Res.*, 2018, **12**(2), 027102.
12 S. Das and M. Pal, Non-invasive monitoring of human health by exhaled breath analysis: a comprehensive review, *J. Electrochem. Soc.*, 2020, **167**, 037562.
13 H. Zhang, D. Z. Zhang, D. Y. Wang, *et al*, Flexible single-electrode triboelectric nanogenerator with MWCNT-PDMS composite film for environmental energy harvesting and human motion monitoring, *Rare Met.*, 2022, **41**, 3117–3128.
14 H. Zhang, Z. Zhang, R. Y. Mao, *et al*, MoS2-based charge trapping layer enabled triboelectric nanogenerator with assistance of CNN-GRU model for intelligent perception, *Nano Energy*, 2024, **127**, 109753.
15 L. Zheng, L. L. Wang and G. Z. Shen, Recent Advances in Smart Wearable Sensing Systems, *Adv. Mater. Technol.*, 2018, **3**(12), 1800444.
16 A. T. Guntner, S. Abegg, K. Konigstein, P. A. Gerber, A. Schmidt-Trucksass and S. E. Pratsinis, Breath sensors for health monitoring, *ACS Sens.*, 2019, **4**, 268–280.
17 F. Ke, Q. Zhang, L. Ji, *et al.*, Electrostatic adhesion of polyaniline on carboxylated polyacrylonitrile fabric for high-performance wearable ammonia sensor, *Compos. Commun.*, 2021, **27**, 100817.
18 S. F. Peng, D. C. Xie, J. Wang, M. Q. Chen and L. Xu, Integration of SnO_2 nanoparticles with micro-hot platform for low-power-consumption gas sensors, *Sens. Mater.*, 2018, **30**, 2679–2692.
19 J. H. Kim, Q. Zhou and J. Chang, Suspended graphene-based gas sensor with 1-mW energy consumption, *Micromachines*, 2017, **8**(2), 44.
20 T. C. Wu, A. De Luca, Q. Y. Zhong, X. X. Zhu, O. Ogbeide, D. S. Um, G. H. Hu, T. Albrow-Owen, F. Udrea and T. Hasan, Inkjet-printed CMOS-integrated graphene metal oxide sensors for breath analysis, *npj 2D Mater. Appl.*, 2019, **3**, 42.
21 W. C. Shen, P. J. Shih, Y. C. Tsai, C. C. Hsu and C. L. Dai, Low-Concentration NH_3 Sensors Manufactured Using the CMOS–MEMS Technique, *Micromachines*, 2020, **11**, 92.
22 X. Y. Shao, D. Z. Zhang, M. C. Tang, *et al*, Amorphous Ag catalytic layer-SnO_2 sensitive layer-graphite carbon nitride electron supply layer synergy-enhanced hydrogen gas sensor, *Chem. Eng. J.*, 2024, **495**, 153676.
23 X. Shao, D. Zhang, M. Tang, H. Zhang, Z. Wang, P. Jia and J. Zhai, Amorphous Ag catalytic layer-SnO_2 sensitive layer-graphite carbon nitride electron supply layer synergy-enhanced hydrogen gas sensor, *Chem. Eng. J.*, 2024, **495**, 153676.
24 M. Das and D. Sarkar, One-pot synthesis of zinc oxide - polyaniline nanocomposite for fabrication of efficient room temperature NH_3 sensor, *Ceram. Int.*, 2017, **43**, 11123–11131.
25 D. Zhang, J. Liu and B. Xia, Layer-by-Layer Self-Assembly of Zinc Oxide/Graphene Oxide Hybrid Toward Ultrasensitive Humidity Sensing, *IEEE Electron Device Lett.*, 2016, **37**(7), 916–919.
26 S. Wang, J. Ma, Z. Li, H. Q. Su, N. R. Alkurd, W. Zhou, *et al*, Surface acoustic wave NH_3 sensor based on ZnO/SiO_2 composite film, *J. Hazard. Mater.*, 2015, **285**, 368–374.
27 V. T. Le, T. N. L. Le and V. H. Nguyen, Comparative study of gas sensor performance of SnO_2 nanowires and their hierarchical nanostructures, *Sens. Actuators, B*, 2010, **150**(1), 112–119.
28 Y. Wang, Q. Mu, G. Wang, *et al*, Sensing characterization to NH_3 of nanocrystalline Sb-doped SnO_2 synthesized by a nonaqueous sol-gel route, *Sens. Actuators, B*, 2010, **145**(2), 847–853.
29 G. N. Chaudhari, S. V. Jagtap, N. N. Gedam, M. J. Pawar and V. S. Sangawar, Sol-gel synthesized semiconducting $LaCo_{0.8}Fe_{0.2}O_3$-based powder for thick film NH_3 gas sensor, *Talanta*, 2009, **78**(3), 1136–1140.
30 Y. Shi, L. Peng, Y. Ding, Y. Zhao and G. Yu, Nanostructured conductive polymers for advanced energy storage, *Chem. Soc. Rev.*, 2015, **44**, 6684–6696.
31 T. Someya, Z. Bao and G. G. Malliaras, The rise of plastic bioelectronics, *Nature*, 2016, **540**, 379.

32 H. Yuk, B. Lu and X. Zhao, Hydrogel bioelectronics, *Chem. Soc. Rev.*, 2019, **48**, 1642–1667.
33 P. G. Su, C. T. Lee and C. Y. Chou, Flexible NH_3 sensors fabricated by in situ self-assembly of polypyrrole, *Talanta*, 2009, **80**(2), 763–769.
34 S. K. Gautam and S. Panda, Highly sensitive Cu-ethylenediamine/PANI composite sensor for NH_3 detection at room temperature, *Talanta*, 2023, **258**, 124418.
35 J. Cai, C. Zhang, A. Khan, C. Liang and W. Li, Highly transparent and flexible polyaniline mesh sensor for chemo resistive sensing of NH_3, *RSC Adv.*, 2018, **8**(10), 5312–5320.
36 W. Chen, P. Yang, W. Shen, *et al*, Flexible room temperature ammonia gas sensor based on in-suit polymerized PANI/PVDF porous composite film, *J. Mater. Sci.: Mater. Electron.*, 2020, **31**(14), 11870–11877.
37 P. Dipak, D. C. Tiwari, A. Samadhiya, *et al*, Synthesis of polyaniline (printable nano ink) gas sensor for the detection of ammonia gas, *J. Mater. Sci.: Mater. Electron.*, 2020, **31**(35), 1–10.
38 R. G. Khanapure, A. A. Ghanwat, S. K. Awate, *et al*, Room-temperature ammonia gas sensor based on carboxylic acid-doped polyaniline, *Polym. Bull.*, 2023, **80**, 3183–3195.
39 J. Ding, F. Liu, C. L. Qi, *et al*, Enhanced photoactivity of perovskite Bi_4NbO_8Cl/PTC-NH_2 heterojunction and its application for photoelectrochemical sensing of DNA hydroxymethylation, *Sens. Actuators, B*, 2021, **344**, 130211.
40 C. Zhu, Y. Xu, T. Zhou, *et al*, Self-assembly polyaniline films for the high-performance ammonia gas sensor, *Sens. Actuators, B*, 2022, **365**, 131928.
41 S. Li, A. Liu, Z. Yang, J. He, J. Wang, F. Liu, *et al.*, Room temperature gas sensor based on tin dioxide@ polyaniline nanocomposite assembled on flexible substrate: ppb-level detection of NH_3, *Sens. Actuators, B*, 2019, **299**, 126970.
42 R. S. Ganesh, E. Durgadevi, M. Navaneethan, *et al*, Low-temperature NH_3 sensor based on Mn-doped ZnO nanoparticle decorated microspheres, *J. Alloys Compd.*, 2017, **721**, 182–190.
43 B. Shen, F. Li, Y. Xie, *et al*, High-performance ammonia gas sensor based on GaN honeycomb nanonetwork, *Sens. Actuators, A*, 2020, **312**, 112172.
44 M. Deshwal and A. Arora, Enhanced acetone detection using Au doped ZnO thin film sensor, *J. Mater. Sci.:Mater. Electron.*, 2018, **29**, 15315–15320.
45 D. Degler, S. Rank, S. Mueller, *et al*, Gold-loaded tin dioxide gas sensing materials: mechanistic insights and the role of gold dispersion, *ACS Sens.*, 2016, **1**, 1322–1329.
46 K. Ikeda, K. Takahashi, T. Masuda, H. Kobori, M. Kanehara, T. Teranishi, *et al*, Structural tuning of optical antenna properties for plasmonic enhancement of photocurrent generation on a molecular monolayer system, *J. Phys. Chem. C*, 2012, **116**, 20806–20811.
47 M. B. Gumpu, N. Nesakumar, S. Sethuraman, U. M. Krishnan and J. B. Rayappan, Development of electrochemical biosensor with ceria-PANI core-shell nano-interface for the detection of histamine, *Sens. Actuators, B*, 2014, **199**, 330–338.
48 L. Kumar, I. Rawal, A. Kaur and S. Annapoorni, Flexible room temperature NH_3 sensor based on polyaniline, *Sens. Actuators, B*, 2017, **40**, 408–416.
49 Y. F. Chen, C. Li, X. L. Ma, Q. P. Qiang, B. T. Liu, S. X. Cao, *et al*, Interface defect engineering induced drastic sensing performance enhancement of $W_{18}O_{49}$@PANI nanowires for NH_3 detection at room temperature, *Appl. Surf. Sci.*, 2020, **506**, 144816.
50 T. Li, W. Zeng and Z. Wang, Quasi-one-dimensional metal-oxide-based heterostructural gas-sensing materials: a review, *Sens. Actuators, B*, 2015, **221**, 1570–1585.
51 G. Williams, G. S. V Coles and S. Park, Gas sensing properties of nanocrystalline metal oxide powders produced by a laser evaporation technique, *J. Mater. Chem.*, 1998, **8**, 1657–1664.
52 A. Choudhury, Polyaniline/silver nanocomposites: dielectric properties and ethanol vapor sensitivity, *Sens. Actuators, B*, 2009, **138**, 318–325.
53 A. A. Athawale and S. V. Bhagwat, Synthesis and characterization of novel copper/polyaniline nanocomposite and application as a catalyst in the Wacker oxidation reaction, *J. Appl. Polym. Sci.*, 2003, **89**, 2412–2417.
54 C. Van Tuan, M. A. Tuan, N. Van Hieu and T. Trung, Electrochemical synthesis of polyaniline nanowires on Pt interdigitated microelectrode for room temperature NH_3 gas sensor application, *Curr. Appl. Phys.*, 2012, **12**, 1011–1016.
55 Y. Wang, B. Zhang, J. Liu, *et al*, Au-loaded Mesoporous WO_3 Preparation and n-Butanol Sensing Performances, *Sens. Actuators, B*, 2016, **236**, 67–76.
56 X. Li, X. Zhou, H. Guo, *et al*, Design of Au@ZnO yolk-shell nanospheres with enhanced gas sensing properties, *ACS Appl. Mater. Interfaces*, 2016, **6**(21), 18661–18667.
57 S. Zhang, P. Song, H. Yan, *et al*, Self-assembled hierarchical Au-loaded In_2O_3 hollow microspheres with superior ethanol sensing properties, *Sens. Actuators, B*, 2016, **231**, 245–255.
58 V. Kumar, V. Patil, A. Apte, *et al*, Ultrasensitive Gold Nanostar–Polyaniline Composite for Ammonia Gas Sensing, *Langmuir*, 2015, **31**(48), 13247–13256.
59 H. Yan, P. Song, S. Zhang, J. Zhang, Zh. Yang and Q. Wang, A low-temperature gas sensor based on Au-loaded MoS_2 hierarchical nanostructures for detecting ammonia, *Ceram. Int.*, 2016, **42**(7), 9327–9331.
60 M. S. Nam, J. Y. Kim, A. Mirzaei, M. H. Lee, H. W. Kim and S. S. Kim, Au, and Pt decorated $Ti_3C_2T_x$ MXenes for preparing self-heated and flexible NH_3 gas sensors, *Sens. Actuators, B*, 2024, **403**, 135112.